Synchrotron X-ray pair distribution function analysis of tricalcium silicate pastes

Ana Cuesta[1,a], Jesus D. Zea-Garcia[1,b], Angeles G. De la Torre [1,c], Isabel Santacruz[1,d], Miguel A.G. Aranda[2,1,e]

[1]*Departamento de Química Inorgánica, Cristalografía y Mineralogía, Universidad de Malaga, Malaga/Malaga, Spain*

[2]*Experiments Division, Alba Synchrotron, CERDANYOLA DEL VALLES/ BARCELONA, Spain*

[a]a_cuesta@uma.es
[b]jdavidzea@uma.es
[c]mgd@uma.es
[d]isantacruz@uma.es
[e]g_aranda@uma.es

ABSTRACT

The analysis of nanocrystalline and amorphous components within cement pastes that contain high amounts of crystalline phases is very challenging. Synchrotron powder diffraction jointly with the pair distribution function (PDF) methodology is very useful to characterize complex cement pastes. PDF data can give information about the local structure and bonding environments of the non-crystalline components such as aluminate hydrate and calcium-(aluminum)-silicate-hydrate gels. The main goal of this work is to characterize amorphous and nanocrystalline gels which are present in cementitious pastes by total scattering PDF analyses in selected real-space ranges. Moreover, the PDF approach also allows quantitatively determining the nanocrystalline and microcrystalline contents.

Several sets of tricalcium silicate pastes have been studied and the results are reported: (i) pastes from different tricalcium silicate polymorphs, such as monoclinic and triclinic; and (ii) the influence of selected parameters in triclinic tricalcium silicate pastes. For all the PDF analyses, a multi r-range approach was followed: the higher r-range (≈40 – 70 Å) is used to determine the microcrystalline phase contents, portlandite and unreactive alite; then, the intermedium r-range (≈10 – 25 Å) allows characterizing the atomic ordering in the nanocrystalline fraction of the C-S-H gel; and finally, the low r-range, below ≈10 Å, gives insight about the chemical nature of the additional amorphous component.

It was concluded that for all the untreated tricalcium silicate pastes, the crystal structure of tobermorite-11 Å fits the nanocrystalline contribution of the C-S-H gel in the 10 – 25 Å r-region much better than tobermorite-14 Å.

1. INTRODUCTION

The hydration reactions of cement samples lead to the precipitation of crystalline materials jointly with nanocrystalline and amorphous gels (Taylor, 1997). The characterization of the nanocrystalline/amorphous gels is very challenging but the presence of large amounts of crystalline phases in the mixtures makes this type of analysis even more complicated.

Rietveld methodology allows to study the crystal structures of microcrystalline phases and also to quantitatively determine their contents. The overall amount of amorphous and non-crystalline content can also be estimated by using the Rietveld method jointly with the internal (De La Torre et al., 2001) or external (Jansen et al., 2011) standard methodologies, although these methodologies do not provide information about the atomic ordering in these non-crystalline phases. High-energy synchrotron X-ray scattering jointly with the pair distribution function (PDF) methodology is very useful to deeply study complex cement pastes. PDF data provide information about the local structure and bonding environments of the nanocrystalline and amorphous components such as cement gels (Cuesta et al. 2017a, b; Cuesta et al., 2018) .

The PDF function, G(r), shows the probability of finding pairs of atoms separated by a distance r. G(r) can be obtained by a Fourier transform of the total scattering powder diffraction pattern, see equation (1) (Billinge & Kanatzidis 2004; Skinner et al. 2010).

$$\boldsymbol{G(r) = 4\pi r[\rho(r) - \rho_0] = \frac{2}{\pi}\int_0^\infty Q[S(Q) - 1]\sin(Qr)dQ} \quad (1)$$

where ρ(r) is the microscopic atomic pair density, ρ_0 is the average atomic number density, S(Q) is the total scattering structure function and Q is the momentum transfer (Billinge & Kanatzidis 2004), $Q=4\pi\sin(\theta)/\lambda$. The quality of the PDF pattern is directly related with the Q-range, which has to be large enough to solve the low-r region peaks. This is the reason why it is needed to use a short wavelength and high 2θ diffracting angles with good signal-to-noise ratio and free from systematic errors (White et al. 2015).

This PDF approach, using synchrotron radiation (Proffen et al., 2005), has been applied in the characterization of different cement samples (Aranda, 2016). Firstly, the local structure of the main gel present in OPC cement, C-S-H, has been thoroughly studied. Some authors have hydrated tricalcium silicate to study the C-S-H gel precipitated in this reaction (Skinner et al., 2010; White, 2016; White et al., 2015). However, directly synthesized pure C-S-H gel have also been widely studied by PDF (Grangeon et al., 2017; Morandeau & White, 2015; Soyer-Uzun et al., 2012) in order to avoid/minimize the contribution of crystalline phases such as unreacted tricalcium silicate and crystalline portlandite. The main conclusion of these studies is that the C-S-H gel has a nanocrystalline nature with an atomic ordering close to 4 nm (Skinner et al., 2010; White, 2016; White et al., 2015). At this point it is important to highlight that the C-S-H gel obtained from the hydration of alite is reported to contain at least two components: a nanocrystalline defective clinotobermorite, $Ca_{11}Si_9O_{28}(OH)_2 \cdot 8.5H_2O$ and an amorphous component which seems to be monolayers of calcium hydroxide (Cuesta et al. 2018; Grangeon et al. 2017). The strategy followed to analyse the cement pastes was the multi r-range analysis approach. For the tricalcium silicate hydrated samples, the ~4-7 nm r-range allowed determining the crystalline phase contents, then, the ~1-2.5 nm r-range was used to characterize the atomic ordering in the nanocrystalline gel; and the ~0.2-1.0 nm r-range gives information about amorphous components (Cuesta et al. 2017b; Cuesta et al. 2018). Recently, the PDF study of C-A-S-H and C-(N)-A-S-H gels (White et al. 2015) have been carried out to highlight the differences between nanocrystalline C-A-S-H gel and amorphous C-(N)-A-S-H gel.

Aluminium hydroxide (A-H) gels resulting from ye'elimite-containing pastes were also studied by the PDF methodology. It was found that the aluminium hydroxide gel had a gibbsite-type local structure with a particle size close to 3 nm (Cuesta et al. 2017b). A similar A-H gel was characterized in calcium aluminate-containing pastes and in this system the A-H gel presented larger particle sizes, between 5-7 nm (Cuesta et al., 2017a; Cuesta et al., 2017b). Finally, other amorphous cement systems were also characterized by this methodology, for instance, geopolymers (Meral et al. 2011; White et al. 2013) and fly ash (Natali et al., 2016).

The main aim of this study is to use total scattering synchrotron data analysed by PDF methodology in order to study the local structures of the different component in alite pastes. For instance, triclinic and monoclinic tricalcium silicates were hydrated under a range of conditions.

2. MATERIALS AND METHODS

2.1 Sample preparation

Monoclinic and triclinic tricalcium silicates, C_3S, have been purchased from Mineral Research Processing (M.R.PRO). Alite samples have been hydrated using two different methodologies:

- *In-situ* hydration: pastes were made by hand-mixing the corresponding sample with the adequate amount of twice boiled demineralised water in a small plastic beaker for 2 min with a spatula and then immediately loaded into glass capillaries of 0.7 mm of diameter with a syringe. The capillaries were sealed with grease to avoid water loss. The capillaries were rotated for one day. Finally, capillaries were kept inside closed plastic containers for about two months. It is highlighted that the hydration reactions were not arrested. Three samples were prepared by using this methodology:

  - Monoclinic C_3S hydrated at RT using a water-to-solid mass (w/s) ratio of 0.5. This sample is labelled as: C_3Sm_050_RT.
  - Triclinic C_3S hydrated at RT using a w/s ratio of 0.5. This sample is labelled as: C_3St_050_RT.
  - Triclinic C_3S hydrated at 35ºC using a w/s ratio of 0.5. This sample is labelled as: C_3St_050_35ºC

- Ex-situ hydration: pastes, prepared as previously described, were poured into hermetically closed Teflon® cylinder shaped moulds for three days (García-Maté et al., 2015). Then, samples were taken out and stored within demineralised and twice boiled water. Pieces were extracted after approximately two months of hydration. At this stage, the pastes were milled to fine powder in an agate mortar. To remove the unreacted water and to arrest the hydration reaction, samples were filtered in a Whatman system (90 mm diameter Whatman filter with a pore size of 2.5 µm on a Teflon support) and washed twice with isopropanol and finally once with ether. Then, the glass capillaries were filled with these powders. Two samples were prepared by using this methodology:

  - Triclinic C_3S hydrated at RT using a w/s ratio of 0.5. This sample is labelled as: C_3St_050_RT_stop
  - Triclinic C_3S hydrated at 50ºC using a w/s ratio of 0.5. This sample is labelled as: C_3St_050_50ºC_stop

2.2 Synchrotron X-ray scattering

High-energy synchrotron X-ray scattering data were collected at the ID15A beamline at the ESRF, Grenoble (France). The selected beam energy was 65.341 keV, λ=0.18972(1) Å. The beam was monochromatised by a double bent Laue monochromator resulting in an energy band pass of ca. 4×10^{-3} $\Delta E/E$. The used detector was a CdTe Pilatus-2M with 172 µm of pixel size. The beamsize was 100 µm horizontal and 100 µm vertical. The detector was off-centred with respect to the incident beam and located very close to the sample, to access up to Q_{inst} = 30 $Å^{-1}$ to calculate the pair distribution function G(r) with very good resolution. CeO_2 standard was used to calibrate the sample-detector distance that was found to be 181.59 mm. The intensity profiles were corrected for the background contribution, polarization of the X-rays and detector geometry, response, and transparency with local software. For each sample, eight frames were collected with acquisition time of 8 s each. So, the total acquisition time was close to 1 minute per sample. The diameter of the glass capillaries was 0.7 mm and they were rotated during data collection to improve diffracting particle statistics.

2.3 Laboratory X-ray powder diffraction (LXRPD)

LXRPD data for selected pastes within capillaries were collected on a D8 ADVANCE (Bruker AXS) diffractometer (SCAI – Universidad de Malaga) equipped with a Johansson monochromator, using

strictly monochromatic Mo-$K\alpha_1$ radiation, λ=0.7093 Å, in transmission geometry (θ/θ). An overall measurement time of ~ 13h per pattern was selected over the angular range 2.8 - 30.0° (2θ) with a 0.020° step size.

2.4 Pair distribution function data analysis

PDF experimental data, G(r), were obtained by using PDFgetX3 (Juhas et al., 2013) with Qmax = 24 $Å^{-1}$. Structural and quantitative phase analysis information was obtained from the PDF data by using the PDFgui software (Farrow et al., 2007). The global optimized parameters were the scale factors, unit cell parameters and atomic displacement parameters (ADPs). The instrumental parameters were obtained by measuring a similar data set for crystalline nickel. In the nickel PDF data analysis, the refined parameters converged to Qdamp = 0.022 $Å^{-1}$ and Qbroad = 0.014 $Å^{-1}$.

2.5 Particle Size Distribution (PSD)

Average particle size and particle size distribution for the alite samples were measured using a laser analyzer (Mastersizer S, Malvern, UK)

3. RESULTS AND DISCUSSION

3.1 *In-situ* hydration: effect of polymorphism of tricalcium silicate on hydration at RT

The particle size distribution (PSD) was measured by using a laser diffraction analyser. For triclinic C_3S, the following values were obtained: $d_{v,10}$=0.8 µm, $d_{v,50}$=4.6 µm and $d_{v,90}$=11.0 µm. For monoclinic C_3S, the obtained values were $d_{v,10}$=0.9 µm, $d_{v,50}$=6.3 µm and $d_{v,90}$=25.6 µm.

Firstly, PDF data for anhydrous triclinic and monoclinic C_3S were collected in identical experimental conditions than hydrated samples. These data were refined over a large r region, i.e. 2 to 50 Å. The resulting structural description was used to fit its contribution in the hydrated pastes (unreacted fraction). For the triclinic sample, the final R_W value was 11.1%. The unit cell values converged to a=11.611 Å, b=14.182 Å, c=13.625 Å, α=104.8º, β=94.5º and γ=90.1. The final ADPs values were 0.0054, 0.0050 and 0.0155 $Å^2$ for Ca, Si and O, respectively. For the monoclinic sample, the final R_W value was 18.2%. The unit cell values converged to a=12.224 Å, b=7.041 Å, c=9.257 Å and β=115.9º and the final ADPs values were 0.0175, 0.0112, and 0.0647 $Å^2$ for Ca, Si and O, respectively. The positional parameters were not optimized.

The full PDF data for alite pastes are very complex due to the presence of different phases of different natures: crystalline (e.g. portlandite and unreacted C_3S), nanocrystalline (e.g. C-S-H gel) and possibly amorphous phase(s). So, after a first inspection, see Figure 1, all the PDF patterns for the hydrated samples were analysed using the previously reported strategy (Cuesta et al. 2017b, Cuesta et al. 2018). In summary, this methodology consists on analysing the large interatomic distance range, here 40-70 Å, for establishing the crystalline phase contents, mainly alite and portlandite, and then to analyse the medium interatomic distance range, here 10-25 Å, for establishing the nanocrystalline phase contents, i.e. the nanocrystalline contribution of the C-S-H gel.

For the hydrated triclinic C_3S, $C_3St\_050\_RT$ as an example, the PDF data were taken at 56 days of hydration. As it was previously reported (Cuesta et al. 2017b, Cuesta et al. 2018), the 40-70 Å region was used to fit the contributions to the PDF pattern of portlandite and unreacted alite, see Figure 2a. The final R_W value converged to 26.7%. Only the scale factor was refined for the unreacted alite. The unit cell values for portlandite converged to a=3.587 Å and c=4.903 Å and the final anisotropic ADP values were u11=u22=0.0043, u33=0.0999 and u12=0.0021 for Ca and u11=u22=0.0091, u33=0.0117 and u12=0.0045 for O. Then, all parameters for crystalline portlandite were kept fixed and the r-region, 10-25 Å, was used to fit the nanocrystalline contribution of C-S-H gel, see Figure 2b. As in previous reports (Cuesta et al. 2017b, Cuesta et al. 2018), two different crystal structures were tested to fit the PDF signal of the gel in this region. Table 1 gives the R_W values for each PDF fit using the selected structural descriptions for the nanocrystalline gel and also includes the quantitative phase analysis results for the different phases. Here, the aim was to distinguish which structure, tobermorite-14 Å (Bonaccorsi et al. 2005) or tobermorite-11 Å (Hamid 1981) gave the best fit for this paste. Jennite was discarded as it was previously reported that jennite yielded poorer fits (Cuesta et al., 2017b). Only a crystal structure for tobermorite-11 Å has been tested here as it was previously reported (Cuesta et al. 2017b) that just small changes can be found between the different crystal structures published for

clinotobermorite or tobermorite-11 Å. As it can be observed in Table 1, the tobermorite-11 Å fits the structure of the nanocrystalline part of the C-S-H gel better than tobermorite-14 Å (i.e. lower R_W factors). In a previous work (Cuesta et al. 2018), it was reported that the scattering misfit of the low r-region, 2 to 10 Å, corresponds to the theoretical PDF trace of isolated monolayers of $Ca(OH)_2$. Consequently, in this work, this low r-region has not thoroughly modelled but it is displayed in Figure 2c.

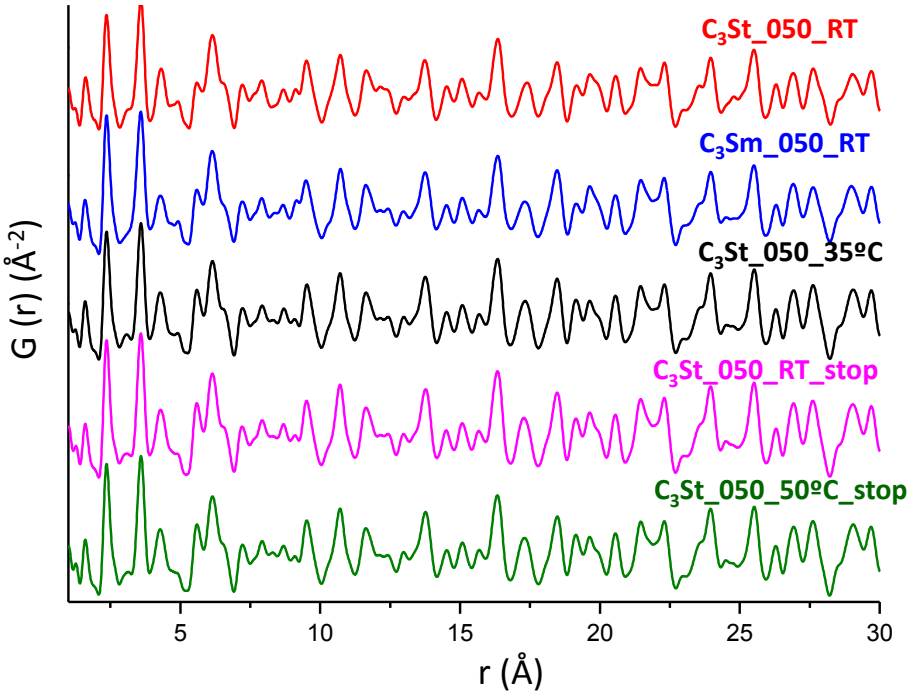

Figure 1. Experimental synchrotron PDF patterns from 1 to 30 Å for the five tricalcium silicate pastes

Table 1. Quantitative phase analysis results obtained by PDF using different crystal structures for the nanocrystalline C-S-H gel. R_W values are also included

sample	Rw (%)	Ca_3SiO_5 (wt%)	$CaCO_3$ (wt%)	Cryst-$Ca(OH)_2$ (wt%)	C-S-H (wt%)
C_3St_050_RT					
Tobermorite-11 (o), ICSD #100405	31.0	30.2	2.2	25.4	42.3
Tobermorite-14 (m), ICSD #152489	34.4	28.9	2.1	24.3	44.7
C_3Sm_050_RT					
Tobermorite-11 (o), ICSD #100405	37.4	26.2	-	25.9	47.9
Tobermorite-14 (m), ICSD #152489	46.1	36.4	-	36.0	27.6
C_3St_050_35ºC					
Tobermorite-11 (o), ICSD #100405	33.5	10.4	3.2	32.1	54.3
Tobermorite-14 (m), ICSD #152489	40.7	9.8	3.0	30.2	57.1
C_3St_050_RT_stop					
Tobermorite-11 (o), ICSD #100405	32.7	14.7	3.5	31.6	50.1
Tobermorite-14 (m), ICSD #152489	35.9	14.0	3.3	30.1	52.6
C_3St_050_50ºC_stop					
Tobermorite-11 (o), ICSD #100405	29.8	-	-	42.3	57.6
Tobermorite-14 (m), ICSD #152489	37.8	-	-	41.9	58.1

*(m) stand for monoclinic and (o) for orthorhombic

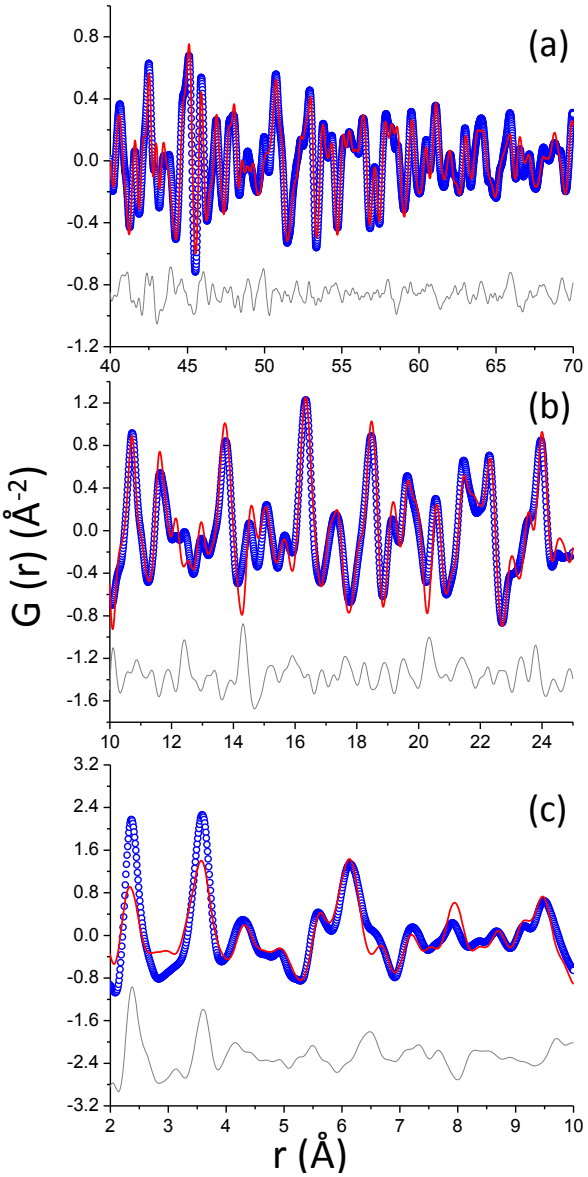

Figure 2. Experimental (blue circles), fitted (red lines) and difference (grey lines) PDF patterns for C_3St_050_RT (a) from 40 to 70 Å; (b) from 10 to 25 Å; and (c) from 2 to 10 Å.

The same strategy was carried out for hydrated monoclinic C_3S, C_3Sm_050_RT. The PDF data were also taken at 56 days of hydration. The contributions to the PDF pattern of portlandite and unreacted alite were studied in the 40-70 Å r-region. The final R_W value in this region converged to 33.5%. The unit cell values for portlandite converged to a=3.587 Å and c=4.904 Å and the final anisotropic ADPs values were u11=u22=0.0071, u33=0.0063 and u12=0.035 for Ca and u11=u22=0.0078, u33=0.0097 and u12=0.0039 for O. Then, the r-region, 10-25 Å, was used to fit the nanocrystalline contribution of C-S-H gel. Table 1 shows the R_W values for each PDF fit using the selected structural descriptions for the nanocrystalline gel and also includes the quantitative phase analysis results for the different phases. Again, for the monoclinic sample, the crystal structure of tobermorite-11 Å fits the nanocrystalline contribution of the C-S-H gel better than tobermorite-14 Å. Figure 3 shows the PDF fit in the 10-25 Å r-region to compare both tobermorites. It is clear that some peaks are worst fitted by using the crystal structure of tobermorite 14 Å (arrows in Figure 3-right).

It can be observed that the crystal structure of tobermorite-11 Å is the best option to fit the nanocrystalline contribution of the C-S-H gel for both C_3S pastes, triclinic and monoclinic (hydrated with the in-situ procedure at RT and w/s=0.50). So, it can be derived that there is not a significant influence in the nanocrystalline part of the precipitated gel with the alite polymorphism. However, it is also important to point out that the degree of hydration of the alite samples hydrated inside the

capillaries is low. At 56 days of hydration, there is a considerable amount of unreacted alite in both capillaries.

It is also worth to highlight that in previous works (Cuesta et al. 2017b, Cuesta et al. 2018), different monoclinic C_3S samples were also hydrated by using different procedures, and then studied by the PDF. Two main differences can be found when comparing the results obtained here and the previous reports: (i) the dopants of previous C_3S samples were different, f.i. they contained an important amount of iron oxide and (ii) although the previous pastes were also analysed by the PDF methodology, these data were collected in a different beamline (MSPD beamline at ALBA synchrotron) by using a smaller energy and a higher data acquisition time, close to 3 hours. The Qbroad parameter obtained by using the experimental configuration here is higher than that obtained in the ALBA synchrotron experiments. This fact leads to broader peaks and consequently, a slightly less precise quantitative phase analysis results. A deep study on the comparison of the PDF data acquired at different facilities is out of the scope of this work and will be published elsewhere.

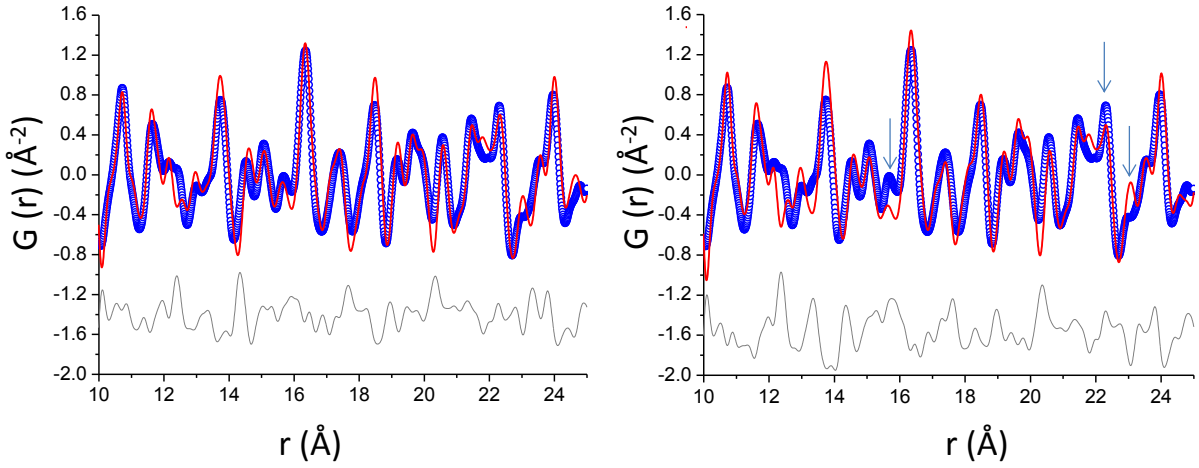

Figure 3. Experimental (blue circles), fitted (red lines) and difference (grey lines) PDF patterns for C_3Sm_050_RT (left) using tobermorite-11 Å and (right) using tobermorite-14Å.

3.2 *In-situ* hydration: effect of temperature on hydration of triclinic tricalcium silicate

The influence of the temperature on the hydration mechanism of triclinic tricalcium silicate was also followed by studying the PDF data. The results for the sample at RT have been described in the previous section. For the C_3St_050_35ºC sample, the PDF data were taken at 63 days of hydration. The final R_W value in the 40-70 Å r-region converged to 28.6%. The unit cell values for portlandite and the final anisotropic ADPs values were similar to that reported for the previous triclinic sample. After keeping fixed the refined parameters for crystalline portlandite and the scale factor for unreacted alite, the nanocrystalline contribution of C-S-H gel was refined in the r-region, 10-25 Å, as previously described. Table 1 also shows the R_W values for each PDF fit by using the two selected structural descriptions for the nanocrystalline gel and also includes the quantitative phase analysis results for the different phases. Again, for C_3St_050_35ºC sample, the crystal structure of tobermorite-11 Å fits the nanocrystalline contribution of the C-S-H gel better than tobermorite-14 Å.

It can be observed that tobermorite-11 Å fits better for both triclinic C_3S pastes, so, there is no significant influence in the local structure of the precipitated C-S-H gel within this temperature range. However, and as expected, the reaction degree in the C_3St_050_35ºC sample is higher than that of the hydrated sample at RT, C_3St_050_RT. This is observed when comparing the amounts of unreacted alite for both pastes, see Table 1.

3.3 Effect of hydration procedure on hydration of triclinic tricalcium silicate at RT

As it was previously described in the materials and methods section, the triclinic C_3S was also hydrated in a cylinder mould and the hydration reaction was stopped after 47 days of hydration. After this step, the hydration-arrested paste was filled within the capillary. This sample was labelled as C_3St_050_RT_stop.

The 40-70 Å region was used to fit the contributions to the PDF pattern of the crystalline phases. The final R_W value in in this r-region converged to 26.0%. The unit cell values for portlandite and the final anisotropic ADPs values were similar to that reported above. Then, the 10-25 Å r-region was used to fit the contribution of the nanocrystalline gel. Again, the crystal structures of tobermorites, 11 Å and 14 Å, were tested, see Table 1. Figure 4 (left) shows the final PDF fit for C_3St_050_RT_stop sample in the 10-25 Å r-region.

It can be observed that for this stopped hydration paste, which was prepared by the *ex-situ* procedure, tobermorite 11 Å fits better the crystal structure of the gel as it was previously observed for the same paste prepared by the *in-situ* procedure. So, it seems that this slightly different hydration procedure and more important, the arresting of the hydration, does not have a significant influence in the local atomic order of the precipitated C-S-H gel.

An important difference between both samples is the degree of reaction, for C_3St_050_RT_stop is larger than that of C_3St_050_RT. This is very likely due to the different hydration methodology. For the *in-situ* hydration, the volume of the paste inside the capillary is much smaller than that inside the cylinder (*ex-situ* hydration). We speculate that in the small capillary, the hydration products which precipitate with time can create passive layers, i.e. hinder the diffusion of ions and water to anhydrous particles, that can avoid the progress of the hydration. In addition, it is not possible to guarantee that all the water which is injected with the syringe is introduced as a whole (and homogenously distributed) inside the capillary. Issues related with inhomogeneous water distribution within small capillaries have been already reported (Gallucci at al., 2007).

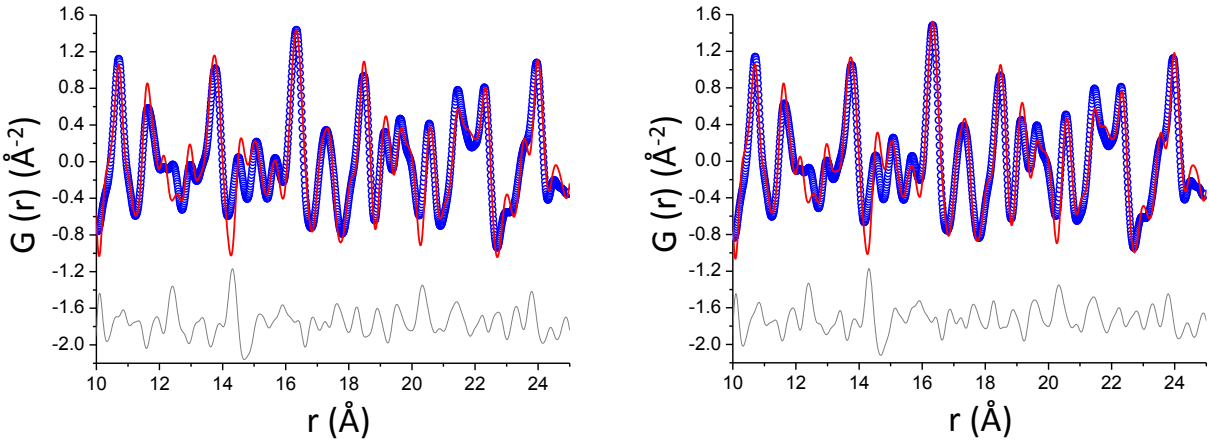

Figure 4. Experimental (blue circles), fitted (red lines) and difference (grey lines) PDF patterns for (left) C_3S_050_RT_stop and (right) C_3S_050_50ºC_stop.

3.4 Ex-situ hydration: effect of temperature on the hydration of triclinic tricalcium silicate.

The influence of the temperature in the hydration mechanism of triclinic C_3S prepared by the *ex-situ* procedure can be also followed by studying the PDF data. The results for the sample hydrated at 50ºC are hereby compared with the sample described above, C_3St_050_RT_stop. For the C_3St_050_50ºC_stop sample, the PDF data were taken at 48 days of hydration. The final R_W value in the 40-70 Å r-region converged to 28.8 %. Table 1 shows the R_W values in the 10-25 Å r-region for each PDF fit using the two selected crystal structures of tobermorite for the fitting of the nanocrystalline gel.

For this sample, there is no unreacted alite because of the high temperature employed in the hydration process. Moreover, the absence of additional unreacted phases leads to a lower R_W value in the 10-25 Å r-region, see Figure 4 (right). It can be also concluded here that the temperature does not significantly affects the local atomic order of the precipitated gel in this temperature range.

3.5 LXRPD study of selected samples.

LXRPD study has been also carried out to double-check the main results derived from the PDF study. Specifically, the LXRPD powder patterns can highlight the presence of tobermorite-11 Å (and even the

absence of tobermorite-14 Å) in these samples. The main difference between both structures can be found in the d-spacing of the (002) reflection of each crystal structure.

The LXRPD patterns for three samples, C_3St_050_RT, C_3St_050_RT_stop and C_3St_050_50ºC_stop, are shown in Figure 5. The low angle region (high d-spacing) allows identifying tobermorite-11 Å and tobermorite-14 Å. The tinny reflection observed at d-spacing 11.48 Å in all the patterns corresponds to tobermorite-11 Å. However, there is no presence of any diffraction signal close to 14.0 Å. So, the LXRPD study also seems to discard the presence of tobermorite-14 Å in the hydration pastes of tricalcium silicate.

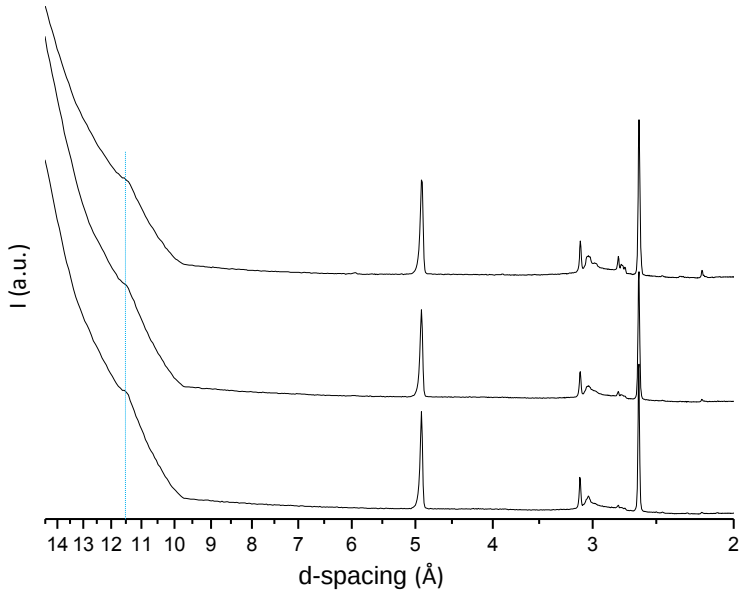

Figure 5. LXRPD patterns for (top) C_3St_050_RT, (medium) C_3St_050_RT_stop and (bottom) C_3St_050_50ºC_stop.

4. CONCLUSIONS

The total scattering synchrotron data analysed by the PDF approach has allowed studying the local atomic order of the C-S-H gel for different tricalcium silicate pastes, prepared by two methodologies. Firstly, it was found that the precipitated C-S-H gel by hydrating two tricalcium silicate polymorphs, monoclinic and triclinic, with the in-situ methodology, had very similar atomic local order. The structural description that better fits the PDF data, in the 10-25 Å r-region, is tobermorite 11 Å. Moreover, the presence of tobermorite 14 Å was discarded in the pastes from both polymorphs. It is noted that hydration was not arrested and there is no evidence of high crystallizing water content in tobermorite (that it should lead to tobermorite 14 Å).

Additionally, it was checked that the local atomic order of the nanocrystalline part of the precipitated C-S-H gel, was not depend on the temperature (in the studied temperature range). This conclusion was drawn as for C_3St_050_35ºC paste, the atomic ordering of tobermorite-11 fits better its PDF data. As expected, the reaction degree for the sample hydrated at 35ºC was higher than that of the hydrated sample at RT.

The samples that were hydrated by the *ex-situ* procedure, C_3St_050_RT_stop and C_3St_050_50ºC_stop, were also studied. It can also be concluded that the hydration procedure and hydration arresting step did not have a significant influence on the local atomic order of the C-S-H gel. For both pastes, tobermorite 11 Å fitted the PDF data of the C-S-H gel better than tobermorite 14 Å. The reaction degree for the sample hydrated at 50ºC was 100% as no unreacted C_3S was identified in the synchrotron total scattering powder pattern.

5. ACKNOWLEDGEMENTS

This work has been supported by Spanish MINECO through BIA2017-82391-R, which is co-funded by FEDER. Authors thank ESRF (Grenoble, France) for providing us with beam time at ID15A beamline.

6. REFERENCES

Aranda, MAG (2016). *Recent studies of cements and concretes by synchrotron radiation crystallographic and cognate methods.* Crystallography Reviews, Volume *22,* Issue 3, pp 150-196.

Billinge, SJL, & Kanatzidis, MG (2004). *Beyond crystallography: the study of disorder, nanocrystallinity and crystallographically challenged materials with pair distribution functions.* Chemical Communications, Volume 0, Issue 7, pp 749-760.

Bonaccorsi, E, Merlino, S, & Kampf, AR (2005). *The crystal structure of tobermorite 14 Å (plombierite), a C-S-H phase.* Journal of the American Ceramic Society, Volume *88, Issue* 3, pp 505-512.

Cuesta, A., Ichikawa, RU, Londono-Zuluaga, D, De la Torre, AG, Santacruz, I, Turrillas, X, & Aranda, MAG. (2017a). *Aluminum hydroxide gel characterization within a calcium aluminate cement paste by combined Pair Distribution Function and Rietveld analyses*. Cement and Concrete Research, Volume 96, pp 1-12.

Cuesta, A, Zea-Garcia, JD, Londono-Zuluaga, D, De la Torre, AG, Santacruz, I, Vallcorba, O., Dappiagi, M, Sanfelix, SG, & Aranda, MAG (2018). *Multiscale understanding of tricalcium silicate hydration reactions*. Scientific Reports, Volume 8, Issue 1, pp 8544.

Cuesta, A, Zea-Garcia, JD, Londono-Zuluaga, D, De La Torre, AG, Santacruz, I, Vallcorba, O, & Aranda, MAG (2017b). *Synchrotron radiation pair distribution function analysis of gels in cements*. Crystals, Volume 7, Issue 10, pp 317.

De La Torre, AG, Bruque, S, & Aranda, MAG (2001). *Rietveld quantitative amorphous content analysis. Journal of Applied Crystallography*, Volume 34, Issue 2, pp 196-202.

Farrow, CL, Juhas, P, Liu, JW, Bryndin, D, Božin, ES, Bloch, J, Proffen, Th, & Billinge, SJL (2007). *PDFfit2 and PDFgui: computer programs for studying nanostructure in crystals*. Journal of Physics: Condensed Matter, Volume 19, Issue 33, pp 335219.

Gallucci, E, Scrivener, K, Groso, A, Stampanoni, M, & Margaritondo, G (2007). *3D experimental investigation of the microstructure of cement pastes using synchrotron X-ray microtomography* (μCT). Cement and Concrete Research, Volume 37, Issue 3, pp 360-368.

García-Maté, M, De La Torre, AG, León-Reina, L, Losilla, ER, Aranda, MAG, & Santacruz, I (2015). *Effect of calcium sulfate source on the hydration of calcium sulfoaluminate eco-cement*. Cement and Concrete Composites, Volume 55, pp 53–61.

Grangeon, S, Fernandez-Martinez, A, Baronnet, A, Marty, N, Poulain, A, Elkaïm, E, Roosz, C, Gaboreau, S, Henocq, P, Claret, F (2017). *Quantitative X-ray pair distribution function analysis of nanocrystalline calcium silicate hydrates: a contribution to the understanding of cement chemistry*. Journal of Applied Crystallography, Volume 50, Issue 1, pp 14–21.

Hamid, SA (1981). *The crystal structure of the 11Å natural tobermorite Ca2.25[Si3O7.5(OH)1.5] · 1H2O*. Zeitschrift Für Kristallographie - Crystalline Materials, Volume 154, pp 3–4.

Jansen, D, Stabler, C, Goetz-Neunhoeffer, F, Dittrich, S, & Neubauer, J (2011). *Does Ordinary Portland Cement contain amorphous phase? A quantitative study using an external standard method*. Powder Diffraction, Volume 26, Issue 01, pp 31-38.

Juhas, P, Davis, T, Farrow, CL, & Billinge, SJL (2013). PDFgetX3: *A rapid and highly automatable*

program for processing powder diffraction data into total scattering pair distribution functions. Journal of Applied Crystallography, Volume 46, pp 560-566.

Meral, C, Benmore, CJ, & Monteiro, PJM. (2011). T*he study of disorder and nanocrystallinity in C–S–H, supplementary cementitious materials and geopolymers using pair distribution function analysis*. Cement and Concrete Research, Volume 41, Issue 7, pp 696-710.

Morandeau, AE, & White, CE (2015). *In situ X-ray pair distribution function analysis of accelerated carbonation of a synthetic calcium–silicate–hydrate gel*. Journal of Materials Chemistry A, Voulem 3, Issue 16, pp 8597-8605.

Natali, ME, White, CE, & Bignozzi, MC (2016). Elucidating the atomic structures of different sources of fly ash using X-ray and neutron PDF analysis. Fuel, Volume 177, pp 148-156.

Proffen, T, Page, KL, McLain, SE, Clausen, B., Darling, TW, TenCate, JA, Lee, S-Y, Ustundag, E (2005). *Atomic pair distribution function analysis of materials containing crystalline and amorphous phases*. Zeitschrift Für Kristallographie - Crystalline Materials, Volume 220, Issue 12, pp 1002-1008.

Skinner, LB, Chae, SR, Benmore, CJ, Wenk, HR, & Monteiro, PJM (2010). *Nanostructure of Calcium Silicate Hydrates in Cements*. Physical Review Letters, Volume 104, Issue 19, pp 195502.

Soyer-Uzun, S, Chae, SR, Benmore, CJ, Wenk, H-R, & Monteiro, PJM. (2012). *Compositional Evolution of Calcium Silicate Hydrate (C-S-H) Structures by Total X-Ray Scattering*. Journal of the American Ceramic Society, Volume 95, Issue 2, pp 793-798.

Taylor, HFW (1997). *Cement chemistry.* Thomas Telford: London, ISBN: 978-0727725929.

White, CE (2016). *Effects of temperature on the atomic structure of synthetic calcium–silicate–deuterate gels: A neutron pair distribution function investigation*. Cement and Concrete Research, Volume 79, pp 93-100.

White, CE, Daemen, LL, Hartl, M, & Page, K. (2015). I*ntrinsic differences in atomic ordering of calcium (alumino)silicate hydrates in conventional and alkali-activated cements*. Cement and Concrete Research, Volume 67, pp 66-73.

White, CE, Page, K, Henson, NJ, & Provis, JL (2013). *In situ synchrotron X-ray pair distribution function analysis of the early stages of gel formation in metakaolin-based geopolymers*. Applied Clay Science, Volume 73, pp 17-25.